

# Computer generation of binary Fresnel holography

Peter Tsang,<sup>1,\*</sup> T.-C. Poon,<sup>2,3</sup> W.-K. Cheung,<sup>1</sup> and J.-P. Liu<sup>3</sup>

<sup>1</sup>Department of Electronic Engineering, City University of Hong Kong, Hong Kong

<sup>2</sup>Bradley Department of Electrical and Computer Engineering, Virginia Tech, USA

<sup>3</sup>Department of Photonics, Feng Chia University, Taiwan

\*Corresponding author: eewmts@cityu.edu.hk

Received 30 July 2010; revised 28 December 2010; accepted 3 January 2011;  
posted 20 January 2011 (Doc. ID 132617); published 28 February 2011

Binarization of Fresnel holograms by direct thresholding based on the polarity of the fringe pattern is studied. It is found that if the hologram is binarized (i.e., for black and white hologram pixels) in this manner, only the edges of the object are preserved in the reconstructed image. To alleviate the errors caused by binarization, the use of error diffusion has been routinely employed. However, the reconstructed image using such standard technique is heavily contaminated with random noise. In this paper, we propose a novel noniterative method for generating Fresnel holograms that are suitable for binarization. Our method is capable of preserving good visual quality on the reconstructed images. © 2011 Optical Society of America

OCIS codes: 090.0090, 090.1760.

## 1. Introduction

Past research in computer-generated holography (CGH) has revealed that a three-dimensional (3D) object scene can be represented with binary instead of gray-scale holograms [1,2]. Such encapsulation allows the holograms to be recorded with smaller data size, and produced swiftly with commodity printers [3], or CD-R [4], which are only capable of outputting black and white dots. For static object scenes, this means of production is substantially lower in cost than the use of a fringe printer [5], and also enables printing of large holograms. In addition, with binary holograms, we could enhance the storage capacity of digital holograms and facilitate more efficient transmission of holograms. However, binarization of the hologram also leads to degradation of the reconstructed image. In the past there were investigations to address the distortions caused by quantization of holograms. These include, for example, the early works of Krishna and Naidu [6], Zhang *et al.* [7], Zhao and Surrel [8], and more recently, Mills

and Yamaguchi [9] on phase-shifting holography, Cable *et al.* [10] on binary Fourier holograms, and Nozaki and Chen [11] and Moreno *et al.* [12] on kinoform and detour phase holograms. Methods for generation of a binary hologram in an iterative manner have been reported in [13–15]. A review of the binarization of holograms is given by Ferri [16]. However, as far as we know, little work has been done on the analysis and generation of binarized Fresnel CGHs in a noniterative manner. This might not be surprising, as we have found that, in general, binarized Fresnel CGHs produce severe distortion upon reconstruction and, if the original object is complicated, there is no discernable reconstruction. Although this problem can be alleviated with error diffusion [17], a method that has been adopted in the binarization of Fourier holograms [18–20], the reconstructed images are contaminated with noise. Apparently this phenomenon is observed when both Fresnel and Fourier holograms are quantized with error diffusion [21]. In this paper we first demonstrate that binarization by direct thresholding on Fresnel holograms will lead to distortion in the form of an edge extracted image of a monochrome image upon holographic reconstruction. We then propose a solution to overcome this problem

---

0003-6935/11/070B88-08\$15.00/0  
© 2011 Optical Society of America

by use of down-sampling of the object before generating the Fresnel hologram.

## 2. Computer Generation and Binarization of Fresnel Holograms

In this section, a brief outline on numerical generation of Fresnel hologram is provided for clarity of presentation. After that, we shall illustrate and explain the distortion caused by binarization of the hologram.

### A. Computer-Generated Holograms [22]

To begin with, given a discrete, planar image  $I(u, v; z_i)$  located at a depth  $z_i$  from a holographic recording plane, a complex Fresnel hologram  $H_F(m, n)$  can be generated numerically as the product of the object wave  $O(m, n; z_i)$  and a planar reference  $R(m, n)$  wave according to Eq. (1a). If the hologram is to be printed on a film, or displayed on an amplitude spatial light modulator (SLM), only the real part of the complex Fresnel hologram is retained, as shown in Eq. (1b):

$$H_F(m, n) = O(m, n; z_i)R^*(m, n), \quad (1a)$$

$$H(m, n) = \text{Re}\{O(m, n; z_i)R^*(m, n)\}, \quad (1b)$$

where  $\text{Re}\{\cdot\}$  represents the real part of a complex number. The object wave is given by

$$O(m, n; z_i) = \sum_{u=0}^{X-1} \sum_{v=0}^{Y-1} I(u, v; z_i) \frac{\exp(ikr(m-u, n-v; z_i))}{r(m-u, n-v; z_i)}, \quad (2)$$

where  $m, u$  and  $n, v$  are the discrete coordinate points along the vertical and horizontal directions, respectively. The term  $r(m-u, n-v; z_i) = \sqrt{(m-u)^2 + (n-v)^2 + z_i^2}$  represents the Euclidean distance between an object point at  $(u, v; z_i)$  and the location  $(m, n)$  on the plane of the hologram.  $X$  and  $Y$  are the vertical and horizontal extents of the image,  $k = 2\pi/\lambda$  is the wavenumber, and  $\lambda$  is the wavelength of the optical beam. All pixels in the image are assumed to be self-illuminating with intensity  $I(u, v; z_i)$ . The reference wave  $R(m, n)$  is assumed to be a plane wave incident at an angle  $\theta$  with respect to the normal of the hologram and hence can be represented by  $R(m)$  for simpler optical geometry.

Equation (2) can be encapsulated as the two-dimensional (2D) convolution of the source image with the Fresnel zone plate  $F(m, n; z_i)$  as [23]

$$O(m, n; z_i) = I(m, n; z_i) * F(m, n; z_i), \quad (3)$$

where  $F(m, n; z_i) = \exp(ikr(m, n; z_i))/r(m, n; z_i)$  and  $*$  denotes a 2D convolution operation involving  $m$  and  $n$ .

Adopting the convolution operation in Eq. (3) in place of Eq. (2), the source image is expressed as a function of  $m$  and  $n$  (i.e.,  $I(m, n; z_i)$ ). The hologram generation process in Eq. (3) can be easily extended to represent a 3D object. The latter is first partitioned into a sequence of evenly spaced planar images positioned at distances  $[z_0, z_1, \dots, z_{N-1}]$  from the hologram. Subsequently, the latter is generated by summing the contribution from each image plane.

### B. Binarization of a Fresnel Hologram

Noniterative binarization of a Fresnel hologram can be realized with direct thresholding, where white and black levels are assigned to hologram pixels with intensity above and below a fixed value, respectively. The process reduces the data size of the hologram as each pixel is only represented with 1 bit. However, it is difficult, if not impossible, to determine a threshold value that will lead to an acceptable reconstructed image for an arbitrary hologram. A more generic means is to binarize a hologram based on the polarity of the pixel (hereafter referred to as "sign binarization"), which is equivalent to setting the threshold value to zero. Although binarizing a hologram in this manner also leads to severe distortion on the reconstructed image, it can retain some edge information of the source image in a lot of cases. The effect is illustrated with the image of a square, as shown in Fig. 1(a), which is placed at a distance of 0.4 m from the hologram. Equation (1a) is applied to generate an on-axis complex Fresnel hologram of the square image with the optical setting listed in Table 1, and the real parts of the hologram before and after binarization are shown in Figs. 1(b) and 1(c), respectively (the imaginary part of the hologram can be inferred in a similar manner).

The reconstructed images of the original and the binarized hologram are shown in Figs. 2(a) and 2(b). It can be seen that, for the latter, only the edge boundary of the square is visible, while the interior content is almost completely removed.

To understand the edge reconstruction shown in Fig. 2(b), let us inspect Figs. 3(a) and 3(b). In Figs. 3(a) and 3(b), we show line traces across the centers of Figs. 1(b) and 1(c), respectively. After applying sign binarization (i.e., setting the threshold value to zero), we see that the high-frequency contents that are located farther away from the center of the graph are emphasized. This emphasis of higher spatial frequencies results in the reconstruction of the edge of the binary object. We also noted that the high frequency fringes at the center region of the graph are removed after thresholding. Although not shown, the imaginary part of the hologram is also subject to the same distortion after binarization. The absence of these fringes results in the missing of the interior shaded area of the reconstructed image.

### C. Explanation of the Effect of Sign Binarization

In this section we shall provide a qualitative explanation of the effect of applying sign binarization on

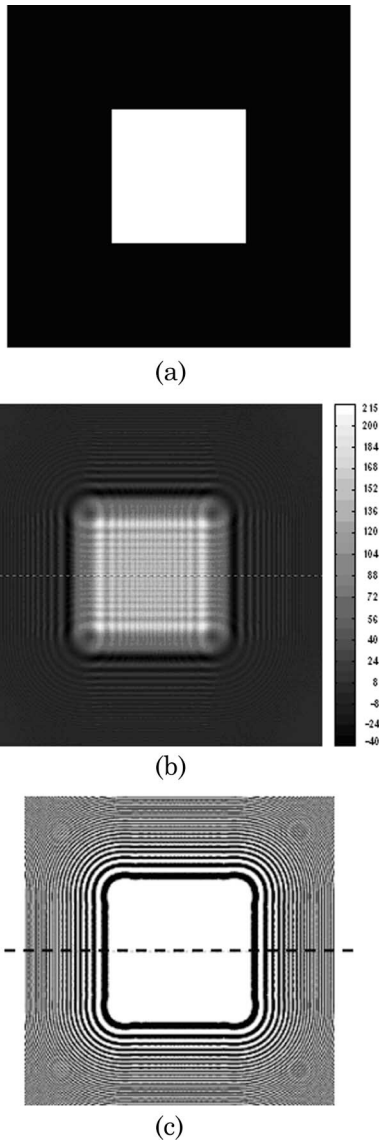


Fig. 1. (a) Intensity image of a solid square positioned at 0.4 m from the hologram. (b) Original hologram (real part of the complex Fresnel hologram based on Eq. (1b) of the solid square. (c) Sign binarization of the real part of the complex Fresnel hologram of the solid square.

the hologram. To begin with, the complex hologram of a single point located at the center of the image plane is generated based on Eq. (1a) and the reconstructed images before and after applying the sign binarization on the hologram are shown in Figs. 4(a) and 4(b), respectively. It can be seen that an individual point is well preserved after the hologram is binarized.

Next, a consecutive sequence of 128 points is juxtaposed into a horizontal line [Fig. 5(a)] and a complex hologram is generated based on Eq. (1a). The reconstructed images before and after applying the sign binarization on the hologram are shown in Figs. 5(b) and 5(c). It can be seen that, after binarization, only the points near the two ends of the line are reconstructed clearly, while the remaining ones are

Table 1. Optical Setting Adopted in the Hologram Generation Process

Hologram size	1024 × 1024 pixels
Pixel size of the hologram	10 μm square
Wavelength of light	650 nm
Illumination angle of reference wave	0°

heavily attenuated in intensity. The reason is that, when individual points are placed closely, their hologram fringes sum up with each other and result in an averaging effect, which weakens the higher-frequency components, while at the same time boosting the low-frequency ones. As a result, the higher-frequency fringes are weakened and may be lost after the sign binarization. It can also be inferred that the pair of points at the left and the right ends of the line are less affected as they have no neighboring points on the right and left sides, respectively. The points at the middle are subjected to larger distortion as they have neighboring points at both sides. This explains why only the edges (i.e., the end points) are preserved in many holograms after the sign binarization.

The points on the line in Fig. 5(a) are evenly separated by a distance of 16 pixels, forming a dotted line, as shown in Fig. 6(a). The reconstructed images of the corresponding hologram before and after the sign binarization are shown in Figs. 6(b) and 6(c), respectively. It can be seen that all the points are reconstructed clearly. The reason is that, when the points are spaced further apart, they retain a higher degree of individualism and are less affected by their neighbors. The averaging effect is smaller and the high-frequency fringes are less attenuated. We also note that increasing the spacing of points is equivalent to down-sampling the original image.

Based on the above observations and explanations, we shall describe, in Section 3, a method for generation of Fresnel holograms that is suitable for sign binarization.

### 3. Proposed Method for Generation of Binary Fresnel Holograms

While it is interesting or perhaps important to have edge information upon reconstruction, sometimes we want to preserve the original image for image display. We propose to solve the aforementioned

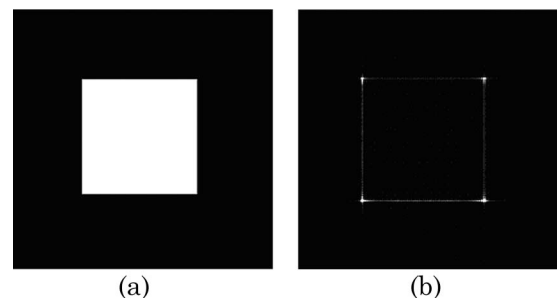


Fig. 2. (a) Reconstructed intensity image of the original hologram in Fig. 1(b). (b) Reconstructed intensity image of the binarized hologram in Fig. 1(c).

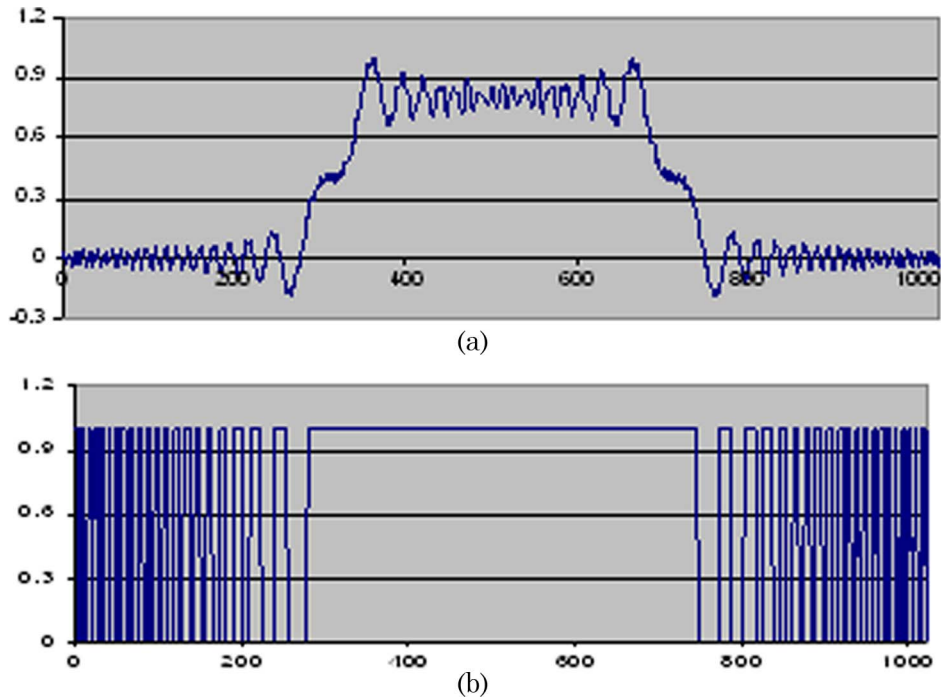


Fig. 3. (Color online) (a) Hologram profile [according to Eqs. (1)] along the horizontal dotted line of the hologram in Fig. 1(b). (b) Hologram profile [according to Eqs. (1a) and (1b)] along the horizontal dotted line of the hologram in Fig. 1(c).

problem with a method for generating a Fresnel hologram that is suitable for binarization. Briefly speaking, we extend the frequency spectrum of the hologram with duplicated images of the baseband signal. This is achieved by down-sampling each image plane  $I(m, n; z_i)$  of a 3D object with a matrix of equally spaced horizontal and vertical grid lines before binarization. The down-sampling image  $I_D(m, n; z_i)$  is represented as follows:

$$I_D(m, n; z_i) = I_1(m, n; z_i) \cup I_2(m, n; z_i), \quad (4)$$

where

$$I_1(m, n; z_i) = \begin{cases} I(m, n; z_i) & m = \tau M \\ 0 & \text{otherwise} \end{cases},$$

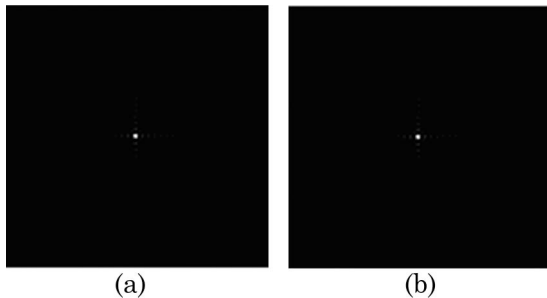


Fig. 4. (a) Reconstructed intensity image of the hologram of a single point. (b) Reconstructed intensity image of the binarized hologram of a single point.

$$I_2(m, n; z_i) = \begin{cases} I(m, n; z_i) & n = \tau M \\ 0 & \text{otherwise} \end{cases},$$

$\tau$  is an integer running from 0,  $\pm 1, \pm 2, \dots$ , and  $M$  is the spacing between adjacent grid lines. The operator  $\cup$  denotes the union of the two sets of data  $I_1(m, n; z_i)$  and  $I_2(m, n; z_i)$ , representing subsampling of  $I_D(m, n; z_i)$  along the  $m$  and  $n$  (i.e., the vertical and horizontal) directions, respectively. Subsampling tends to fill in or strengthen some frequency contents of the hologram before binarization. To clarify it further, let us formulate a single horizontal row of pixels in  $I(m, n; z_i)$  and determine the subsampled signal along the  $m$  direction. For brevity of explanation, we simply express the row of pixels with a one-dimensional representation, i.e., dropping the terms  $n$  and  $z_i$ . After subsampling, the result is given by

$$I_1(m) = I(m) \sum_{r=-\infty}^{\infty} \delta(m - rM). \quad (5)$$

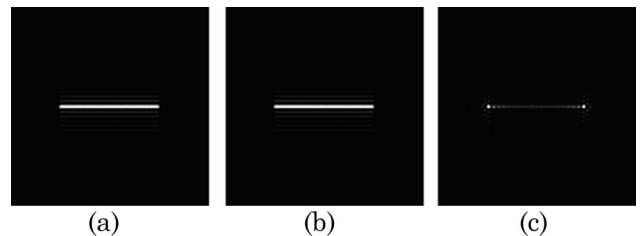


Fig. 5. (a) Line formed by a sequence of 128 points. (b) Reconstructed intensity image of the hologram of the line shown in (a). (c) Reconstructed intensity image of the binarized hologram of the line shown in (a).

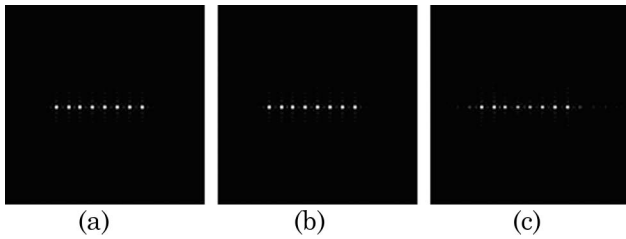


Fig. 6. (a) Dotted line formed by a sequence of eight points with a regular spacing of 16 pixels. (b) Reconstructed intensity image of the hologram of the dotted line shown in (a). (c) Reconstructed intensity image of the binarized hologram of the dotted line shown in (a).

For illustration, we treat  $m$  as a time variable  $t$  and the spectrum of  $I(t)$  with  $f$  as a frequency variable. Figure 7(a) shows the original oversampled signal  $I(t)$  and its spectrum with  $f_S$  as a sampling frequency, which is shown in Fig. 7(b).  $f_A$  denotes the bandwidth of  $I(t)$ . Assuming that the original signal is band limited to avoid aliasing error, the subsampling of the original signal  $I_1$  and its spectrum are shown in Figs. 7(c) and 7(d), respectively, for  $M = 4$ . Note that, for  $M = 4$ , the subsampled signal has four repeated spectra within the range from 0 to  $f_S$ .

After subsampling, because the baseband signal now has been repeated along  $f$ , as shown in Fig. 7(d), this has the effect of filling in some frequencies, namely, those frequencies around  $f_S/M$ ,  $2f_S/M$ , etc., as shown in Fig. 7(d).

To illustrate the effect of subsampling, the square in Fig. 1(a) is down-sampled by 16 times according to Eq. (5). Line traces across the center of the holograms before and after binarization are shown in Figs. 8(a) and 8(b). These line traces can be compared with Figs. 3(a) and 3(b), respectively. We observe noticeably that, in Fig. 8(b), we now have some fringes, albeit binarized, in the center portion of the figure, which are responsible for bringing some of the contents or details back into the original image.

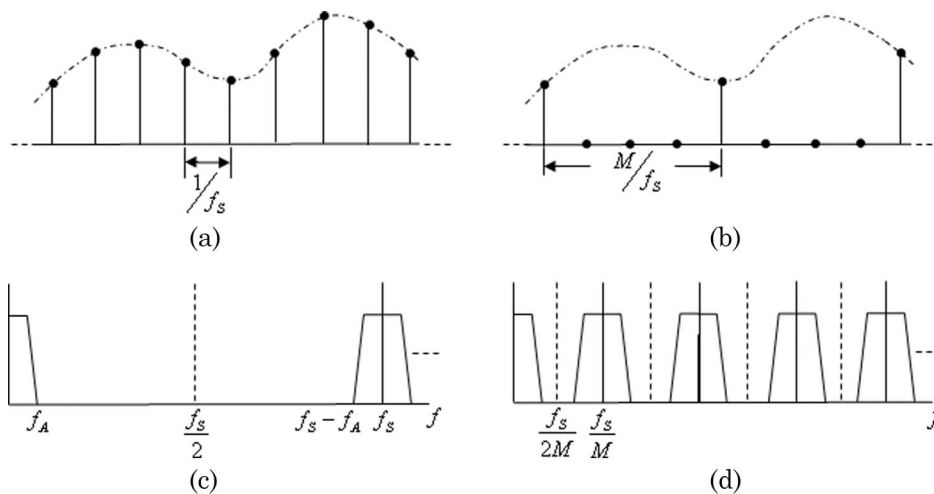


Fig. 7. (a) Original oversampled signal  $I(t)$ . (b) Spectrum of  $I(t)$  with  $f_S$  as a sampling frequency. (c) Subsampling of the original signal  $I_1(t)$ . (d) Spectrum of  $I(t)$  after subsampling by  $M$  times.

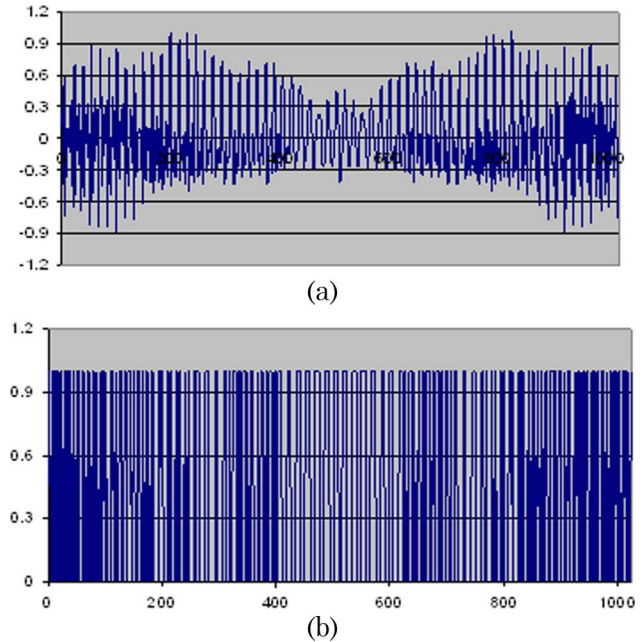


Fig. 8. (Color online) (a) Horizontal line traces across the center of the original hologram of the solid square in Fig. 1(a) after down-sampling by 16 times. (b) Horizontal line traces across the center of the binarized hologram of the solid square in Fig. 1(a) after down-sampling by 16 times.

#### 4. Experimental Evaluation

The white square, as shown in Fig. 1(a), is employed as a source image to demonstrate the performance of our method. The source image is positioned at a distance of 0.3 m from the hologram. Equations (1b) and (2) are applied to generate the off-axis hologram based on the optical setting in Table 2. As the hologram (as well as the rest of the examples in this section) has to be printed on films and optically reconstructed, only the real part of the hologram is retained. In addition, off-axis holograms are prepared to divert the twin image from the viewpoint.

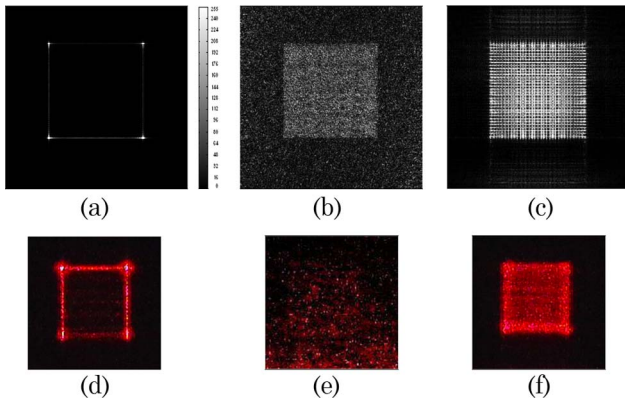


Fig. 9. (Color online) (a) Reconstructed intensity image of the hologram representing the square image in Fig. 1(a), binarized with thresholding. (b) Reconstructed intensity image of the hologram representing the square image in Fig. 1(a), binarized with error diffusion. (c) Reconstructed intensity image of the hologram representing the square image in Fig. 1(a), binarized with our proposed method with a down-sampling factor of 8 on the source image. (d) Optical reconstruction of the intensity image of the binarized (by direct thresholding) hologram of a white square. (e) Optical reconstruction of the intensity image of the binarized (by error diffusion) hologram of a white square. (f) Optical reconstruction of the intensity image of the binarized hologram of a white square being down-sampled by 8 times.

The hologram is then binarized with thresholding (assigning white and black values to positive and negative pixels in the hologram, respectively). Figure 9(a) shows its reconstruction. A gray bar reflecting the correspondence between the intensity and the value is shown in Fig. 9(a). As the same mapping is applied to the rest of the figures on numerical reconstruction, it will not be shown again. In Fig. 9(b), we show the reconstruction after error diffusion has been applied to the binarized hologram. From the figures, it can be seen that binarization with thresholding results in a reconstructed image that removes the interior content of the square and presents the image as a result of edge extraction. With the use of error diffusion, the missing interior region is recovered, but the reconstructed image, as shown in Fig. 9(b), is extremely noisy. Next, we apply our proposed method by down-sampling the source image, based on Eq. (4), with a factor  $M = 8$ . A hologram is generated from the down-sampled image and binarized with thresholding. The reconstructed image is shown in Fig. 9(c). It can be seen that the internal content of the square is preserved, and the visual quality of the reconstructed image is superior to the use of error diffusion. In addition, the noise

Table 2. Optical Setting Adopted in the Experimental Evaluation

Hologram size	1024 × 1024 pixels
Pixel size of the hologram	10 μm square
Wavelength of light	650 nm
Reference wave	Planar
Illumination angle of reference wave	1.2°

Table 3. Comparison of the RMSE Between the Square Image Reconstructed Based on Eq. (1b), and Each of the Binarization Methods

RMSE: Thresholding	RMSE: Error Diffusion	RMSE: Our Proposed Method
131	101	72

contamination is less severe than the result in Fig. 9(b).

The root mean square error (RMSE) between the square image reconstructed without binarization [i.e., based on Eq. (1b)], and the reconstructed image attained with each method, is listed in Table 3. It can be seen that our proposed method results in the smallest RMSE.

To further substantiate our proposed method, we have prepared CGHs for optical reconstruction. The hologram size is about 10.24 mm by 10.24 mm, or 1024 by 1024 points. The hologram is computer generated with the following parameters:  $\lambda = 0.65 \mu\text{m}$ ,  $z_0 = 0.4 \text{ m}$ , with off-axis incident angle of  $\theta = 1.2^\circ$ . All holograms are printed with a printer with 2400 dpi on Agfa Red Sensitive films, and illuminated by a laser beam for optical reconstruction. Figures 9(d)–9(f) show the optical reconstructions for the “square,” which can be compared directly with computer simulation results in Figs. 9(a)–9(c), respectively. In comparing Figs. 9(b) and 9(e), it can be seen that the optical reconstructed images of the hologram that is binarized with error diffusion are significantly poorer than the numerical reconstruction. An explanation is that, with error diffusion, every pixel in the binarized hologram is compensating the errors of its neighbor. When the hologram is printed on the film, there are bound to be some errors imposed by the printer. The error of each hologram pixel propagates to, and also accumulates in other parts of the hologram, hence jeopardizing its effect in compensating the defects of the neighboring pixels. This increases the distortion on the fringe patterns and results in a poorer reconstructed image.

The proposed method is now applied to a 3D source image to demonstrate its usefulness for 3D display. The 3D source image is shown in Fig. 10(a), comprising two lines of text characters. The upper row “CTU” and the lower row “HK” are positioned at a distance of  $z_0 = 0.25 \text{ m}$  and  $z_1 = 0.3 \text{ m}$  from the hologram,

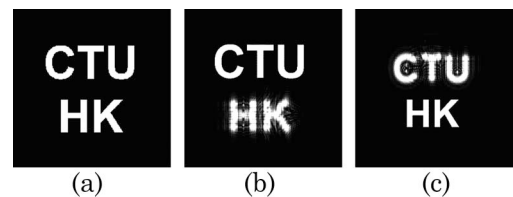


Fig. 10. (a) Source image comprising an upper row of text characters “CTU” at  $z_0 = 0.25 \text{ m}$ , and a lower row of characters “HK” at  $z_1 = 0.3 \text{ m}$ . (b) Reconstructed image of the hologram representing the image in (a), and at  $z_0 = 0.25 \text{ m}$ . (c) Reconstructed image of the hologram representing the image in (a), and at  $z_1 = 0.3 \text{ m}$ .

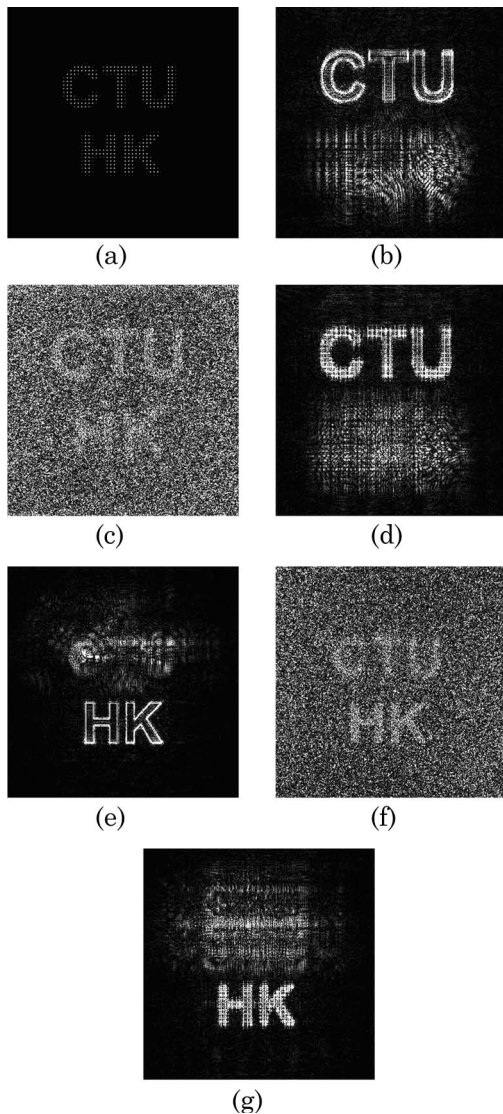


Fig. 11. (a) Source image after applying the antialiasing filter and down-sampling. (b) Reconstructed image at  $z_0 = 0.25$  m of the hologram representing the image in Fig. 10(a), and binarized with thresholding. (c) Reconstructed image at  $z_0 = 0.25$  m of the hologram representing the image in Fig. 10(a), and binarized with error diffusion. (d) Reconstructed image at  $z_0 = 0.25$  m of the hologram representing the image in Fig. 10(a), and binarized with thresholding after subsampling to the source image (our proposed method). (e) Reconstructed image at  $z_1 = 0.3$  m of the hologram representing the image in Fig. 10(a), and binarized with thresholding. (f) Reconstructed image at  $z_1 = 0.3$  m of the hologram representing the image in Fig. 10(a), and binarized with error diffusion. (g) Reconstructed image at  $z_1 = 0.3$  m of the hologram representing the image in Fig. 10(a), and binarized with thresholding after subsampling to the source image (our proposed method).

respectively. The hologram for the source image is generated based on Eqs. (1) and the reconstructed images at  $z_0$  and  $z_1$  are shown in Figs. 10(b) and 10(c), respectively. Next we evaluated the performance obtained with sign thresholding and our proposed method. Note that, when our proposed method is applied, the source image is first filtered with an

Table 4. Comparison of the RMSE Between the “CTU” and the “HK” Images Reconstructed Based on Eq. (1b), and Each of the Binarization Methods

Image	RMSE: Thresholding	RMSE: Error Diffusion	RMSE: Our Proposed Method
“CTU”	71	83	58
“HK”	55	64	43

$8 \times 8$  low-pass mean filter to reduce the aliasing error, followed by down-sampling by 8 times along the horizontal and vertical directions, as shown in Fig. 11(a). The reconstructed images obtained from the hologram binarized with sign thresholding and our proposed method at  $z_0$  and at  $z_1$  are shown in Figs. 11(b)–11(g). For the hologram binarized with thresholding, only the edge boundaries of the text characters are preserved and the interior contents are discarded in the reconstructed images. Both error diffusion and our proposed method are capable of maintaining the interior regions of the images. Apart from a slight blurriness caused by the anti-aliasing filter and the down-sampling process, the visual quality of the reconstructed images obtained by our method is obviously superior to that of error diffusion.

The RMSE between the “CTU” and the “HK” images reconstructed without binarization [i.e., based on Eq. (1b)], and the reconstructed image attained with each method, is listed in Table 4. It can be seen that our proposed method results in the smallest RMSE.

## 5. Conclusion

Binary Fresnel holograms have a number of advantages. First, their data size is smaller as compared with gray-level representation. Second, the holograms can be produced economically and swiftly with commodity printers. Third, as the pixels are bilevel, they are less affected by the nonlinearity characteristics of electronically accessed display devices, such as the SLM. Despite these favorable factors, smooth shaded regions are poorly preserved if a Fresnel hologram is binarized with direct thresholding. We have proposed to adopt a grid line down-sampling scheme to strengthen some of the lost frequency components of the hologram. Experimental evaluation demonstrates the feasibility of the approach, revealing that smooth shaded regions can be reconstructed from binary Fresnel holograms. In addition, as down-sampling is merely a pixel selection process, the overhead it imposes on the computation of the hologram is negligible. We also show that the reconstructed images obtained from holograms binarized by our proposed method is less noisy, and superior in visual quality than that based on error diffusion.

Finally, we want to point out some remarks on our proposed technique. It can be inferred from Eq. (5) and Fig. 7(d) that the higher the down-sampling factor  $M$ , the larger will be the number of repeated

spectra, and the smaller will be the spacing between them. To avoid the aliasing error caused by overlapping of the repeated spectra, the source image has to be band limited with a low-pass filter. As a result, down-sampling the source image  $I(m, n; z_i)$  will contribute to certain degree of blurriness, and also short gaps between adjacent pixels, on the reconstructed image. However, the increase of the down-sampling factor  $M$  will lead to higher diffraction efficiency for optical reconstruction. The optimal choice of  $M$  varies between different object scenes and has to be determined empirically (e.g., via simulation) prior to printing. However, we have found out that a down-sampling factor between 8 and 16 generally results in acceptable visual quality.

## References

1. A. W. Lohmann and D. P. Paris, "Binary Fraunhofer holograms, generated by computer," *Appl. Opt.* **6**, 1739–1748 (1967).
2. B. R. Brown and A. W. Lohmann, "Computer-generated binary holograms," *IBM J. Res. Dev.* **13**, 160–168 (1969).
3. V. Guarnieri and F. Francini, "Computer generated holograms (CGH) realization: the integration of dedicated software tool with digital slides printer," *Proc. SPIE* **3190**, 391–401 (1997).
4. Y. Sakamoto, M. Morishima, and M. A. Usui, "Computer-generated holograms on a CD-R disk," *Proc. SPIE* **5290**, 42–49 (2004).
5. H. Yoshikawa and M. Tachinami, "Development of direct fringe printer for computer-generated holograms," *Proc. SPIE* **5742**, 259–266 (2005).
6. V. V. Krishna and P. S. Naidu, "An overview of quantization in detour phase binary holograms," *Proc. SPIE* **813**, 397–398 (1987).
7. E. Zhang, S. Noehte, C. H. Dietrich, and R. Manner, "Gradual and random binarization of gray-scale holograms," *Appl. Opt.* **34**, 5987–5995 (1995).
8. B. Zhao and Y. Surrel, "Effect of quantization error on the computed phase of phase-shifting measurements," *Appl. Opt.* **36**, 2070–2075 (1997).
9. G. A. Mills and I. Yamaguchi, "Effects of quantization in phase-shifting digital holography," *Appl. Opt.* **44**, 1216–1225 (2005).
10. A. J. Cable, E. Buckley, P. Marsh, N. A. Lawrence, and T. D. Wilkinson, "Real-time binary hologram generation for high-quality video projection applications," in *SID International Symposium Digest of Technical Papers* (2004), pp. 1431–1433.
11. S. Nozaki and Y.-W. Chen, "Evolutionary perturbation of simulated annealing in optimization of kinoforms," in *Fifth International Conference on Natural Computation* (2009), Vol. 6, pp. 13–16.
12. I. Moreno, A. Martínez-García, L. Nieradko, J. Albero, and C. Gorecki, "Low cost production of computer-generated holograms: from design to optical evaluation," *J. Eur. Opt. Soc. Rapid Pub.* **5**, 10011 (2010).
13. M. P. Chang and O. K. Ersoy, "Iterative interlacing error diffusion for synthesis of computer-generated holograms," *Appl. Opt.* **32**, 3122–3129 (1993).
14. E. Zhang, S. Noehte, C. H. Dietrich, and R. Männer, "Gradual and random binarization of gray-scale holograms," *Appl. Opt.* **34**, 5987–5995 (1995).
15. B. B. Chhetri, S. Yang, and T. Shimomura, "Iterative stepwise binarization of digital amplitude holograms with added energy to the signal window," *Opt. Eng.* **40**, 2718–2725 (2001).
16. L. C. Ferri, "Visualization of 3D information with digital holography using laser printers," *Comp. Graph.* **25**, 309–321 (2001).
17. R. W. Floyd and L. Steinberg, "An adaptive algorithm for spatial grey scale," *Proc. Soc. Inf. Display* **17**, 75–77 (1976).
18. R. Eschbach, "Comparison of error diffusion methods for computer-generated holograms," *Appl. Opt.* **30**, 3702–3710 (1991).
19. R. Eschbach and Z. G. Fan, "Complex-valued error diffusion for off-axis computer-generated holograms," *Appl. Opt.* **32**, 3130–3136 (1993).
20. R. L. Easton, R. Eschbach, and R. Nagarajan, "Error diffusion in cell-oriented Fourier-transform computer-generated holograms to compensate for printing constraints," *J. Mod. Opt.* **43**, 1219–1236 (1996).
21. F. Fetthauer, S. Weissbach, and O. Bryngdahl, "Computer-generated Fresnel holograms: quantization with the error diffusion algorithm," *Opt. Commun.* **114**, 230–234 (1995).
22. T.-C. Poon, *Digital Holography and Three-Dimensional Display: Principles and Applications* (Springer, 2006).
23. T.-C. Poon, "On the fundamentals of optical scanning holography," *Am. J. Phys.* **76**, 738–745 (2008).